# Innovative Approach to Load-Settlement Curve for Improved Soil Analysis Using BWM Approach in Disaster Mitigation and Resilient Design

**Gitartha Kalita[1], Palash Jyoti Hazarika[2]**

[1]*Assam Engineering College, Jalukbari, Guwahati, Assam, India 781013, gitartha.kalita56@gmail.com.*

[2]*Assam Engineering College, Jalukbari, Guwahati, Assam, India 781013, pjhaz@rediffmail.com.*

***Abstract*: *Understanding the load transfer behavior at the interface between piles and soil is crucial for ensuring the stability and effectiveness of pile foundations. The allowable load that a pile can bear depends on various factors such as soil type, pile dimensions, and the interaction between the pile and surrounding soil. This study delves into the intricacies of load transfer at the pile-soil interface and proposes an innovative approach to accurately calculate these loads. Drawing upon an extensive review of existing literature for the last 3 decades, six studies presenting load transfer equations were identified as foundational to this research. Load-settlement curves were then generated using Octave software, accommodating a range of pile dimensions and soil types. To further refine load calculations, codes were developed to compute allowable bearing loads based on formulas from the Indian Standard code. Additionally, a decision tree model implemented in Python was utilized to predict the optimal load calculation methods for specific soil and pile conditions. Experimental findings unveiled significant variations in load-bearing capacities across different soil types and pile dimensions. The research further investigates six distinct methods for assessing allowable load—Point by Point Curve, Cubic Root Curve, Hiramaya Curve, Hyperbolic Curve, Krasinski Curve, and Root Curve. Each method was analyzed for its performance in load-settlement behavior, with the Hiramaya Curve emerging as the most conservative and reliable due to its lower allowable load estimates, which offer a higher factor of safety. A significant contribution of this study is the development of a merged curve that synthesizes the strengths of these six methods. This study initially evaluated weightage of each study using Best Worst Method (BWM) and then with the help of weightage a merged load settlement curve is drawn for various soil and various dimensions. The merged curve integrates unique parameters like load-bearing capacities and settlement behaviors, providing a comprehensive load-settlement model applicable across six soil types and five classes of pile dimensions. This tool enhances the accuracy and versatility of pile foundation design, offering geotechnical engineers a robust and adaptable model for a wide range of conditions.*

***Keywords*: Load transfer behavior, Pile-soil interface, Octave software, Best Worst Model, Optimal load calculation methods.**

**(Article history: Received: 5th January 2025 and accepted 29th May 2025)**

## I. INTRODUCTION

Foundations are vital for providing support, stability, and safety to buildings, ensuring compliance with regulations [1]. They can be categorized into shallow and deep foundations, each with its own advantages and limitations, selected based on soil conditions, site characteristics, and structural requirements. Pile foundations, a type of deep foundation, are crucial for transferring loads from structures to deeper, more stable soil or rock layers [2]. Piles, typically made of concrete, steel, or timber, offer increased bearing capacity, stability, resistance to lateral loads, and cost-effectiveness, especially in weak or high-water-table soil conditions [3].

### A. *Load Settlement Behavior*

Pile foundation settlement stems from factors like soil consolidation, pile compression, and elastic pile deformation [4]. Various settlement types include elastic, consolidation, secondary consolidation, differential, tilting, and heave settlement. Understanding these settlements is pivotal for ensuring structural integrity and safety. Immediate settlement, primarily for piles in sand, and consolidation settlement, especially for saturated clay soils, play significant roles. Analyzing settlement behavior aids in predicting settlement, preventing failures, ensuring compliance, and optimizing costs [5-6].

Load transfer in pile-soil systems involves numerous parameters like soil type, pile length, and diameter. Accurately assessing these parameters is challenging but essential for rational pile foundation design [7]. The load-transfer curve, depicting pile-soil interaction, is crucial for evaluating load-settlement response. Various methods, including empirical and numerical approaches, aid in constructing load-settlement curves [8]. Understanding load transfer helps ensure structural stability and longevity. Previous studies have proposed different approaches for analyzing load-settlement curves, considering soil types, pile materials, and installation methods [9-10]. These studies have developed various curve types, including linear, root, trilinear, hyperbolic, point by point, and cubic root curves, each suited to specific soil and pile characteristics as shown in Table I.

DETAILS OF VARIOUS STUDIES RELATED TO LOAD VS SETTLEMENT CURVE

| **Curve** | **Soil type** | **Pile type** | | | **Reference** |
|---|---|---|---|---|---|
| | | ***Material of Construction*** | ***Method of installation*** | ***Mode of Load Transfer*** | |
| Linear curves | Sand (Loose/ Medium/ Dense), Clay (Loose/ Medium/ Dense). | Timber, Steel, Concrete, Composite piles | Driven, Bored, Vibrated, Jetted | Bearing, Friction, Tension | [11] |
| Root curve | Sand ( Loose/ Medium/ Dense) | Timber, Steel, Concrete, Composite piles | Driven | Bearing, Friction, Tension | [12] |
| Linear curves | Fine-grained soil and Coarse-grained soil | Timber, Steel, Concrete, Composite piles | Replacement piles and Driven piles | Bearing, Friction, Tension | [13] |
| Trilinear curves | Sand (Loose/ Medium/ Dense), Clay (Loose/ Medium/ Dense). | Timber, Steel, Concrete, Composite piles | Driven, Bored, Vibrated, Jetted | Bearing, Friction, Tension | [14-15] |
| Hyperbolic curves | Sand (Loose/ Medium/ Dense), Clay (Loose/ Medium/ Dense). | Timber, Steel, Concrete, Composite piles | Driven, Bored, Vibrated, Jetted | Bearing, Friction, Tension | [16] |
| Point by point curves | Clay non-Carbonate sand. | Timber, Steel, Concrete, Composite piles | Driven, Bored, Vibrated, Jetted | Bearing, Friction, Tension | [17] |
| Cubic root curve | Sand (Loose/ Medium/ Dense), Clay (Loose/ Medium/ Dense). | Timber, Steel, Concrete, Composite piles | Driven, Bored, Vibrated, Jetted | Bearing, Friction, Tension | [18] |
| Hyperbolic curve | Sand (Loose/ Medium/ Dense), Clay (Loose/ Medium/ Dense). | Timber, Steel, Concrete, Composite piles | Driven, Bored, Vibrated, Jetted | Bearing, Friction, Tension | [9] |

### B. Literature Review

Coyle and Reese [9] introduced an analytical approach to establish theoretical load-settlement curves for piles loaded in clay, validating their method through both field and laboratory experiments. Poulos and Davis [6] employed Mindlin's equation to examine settlement behavior, emphasizing the prevalence of immediate settlement in ideal soil conditions. Randolph and Wroth [19] developed closed-form solutions for piles loaded vertically in linear elastic soil, while Briaud and Tucker [20] proposed a method for calculating shaft and end resistance in piles driven into sand.

Several researchers, such as Chow [21], Puolos [22], and Polo and Clemente [23], suggested methodologies for predicting settlement, demonstrating favorable agreement with field tests. Kiousis and Elansary [24] introduced a method for assessing load settlement behavior similar to that of Coyle and Reese [9]. They synthesized the load settlement curve at the pile's top by numerically integrating load transfer relationships. Kaniraj [25] derived a semi-empirical equation for settlement ratio in sand, while Zhu and Chang [26] outlined a procedure for t-z curves along bored piles. Recent studies by Bohn et al. [27] and Zhou et al. [28] introduced cubic, hyperbolic, and trilinear load transfer models, enhancing accuracy in load-settlement predictions.

Balakrishnan et al. [29] proposed a methodology for determining load deformation and distribution curves for bored piles in residual weathered formation, incorporating nonlinear behavior of pile material. Kim et al. [30] used load transfer approach to evaluate load distribution and deformation of drilled shafts, proposing a hyperbolic model for shear function. Shen et al. [31] proposed a variational approach for analyzing vertical deformation of pile groups, predicting performance reasonably well. Dyson and Randolph [32] studied the response of piles in calcareous sand under lateral loading, proposing load transfer curves believed to offer an improved approach for pile design. The authors modified two most common methods used in practice, which are described in detail by Reese et al. [33] and the American Petroleum Institute (API) method based on O'Neill and Murchinson [34]. Al-Homoud et al. [35] evaluated the accuracy of prediction models for pile settlement in the UAE, recommending suitable models [36-37] for different loading stages [38]. Results showed that settlement values predicted by Vesic [36] and Poulos [22] overestimated the true values. However, it was observed that Vesic method was less conservative than Poulos method. Mostafa and Naggar (2004) [37] used p-y and t-z curves to study the response of offshore platforms, modeling static and dynamic curves using nonlinear springs and dashpots.

Kim et al. (2007) [39] presented a modified analytical model for analyzing pile axial load capacity, using solid finite elements with nonlinear load transfer curves. Chang and Zhu (2004) [38] developed a methodology to account for stress relief and soaking of boreholes in water, proposing a modulus reduction factor for load transfer curves. Hyeongjoo et al. (2008) [40] demonstrated earth-pile reaction under subsidence conditions using t-z and q-z curves. Chou and Hsiung (2009) [41] developed normalized equations for axially loaded piles based on an elasto-plastic soil model. Bradshaw et al. (2012) [42] interpreted load transfer curves from static load tests on large-diameter pipe piles in silty soils. Lim et al. (2013) [43] presented t-z and q-z curves based on instrumented bored pile in layered soils, using calibrated modulus for accurate load settlement prediction. The developed curve is having a little difference with t-z curve for clay by Reese and O'Neil (1988) [44]. Ismail (2014) [45] calculated load transfer curves from un instrumented pile loading tests using a self-learning algorithm, producing better load deformation models compared to conventional t-z curves. Nanda and Patra (2014) [46] proposed a methodology for determining load transfer and settlement curves, accommodating nonlinear soil stress-strain behavior. Abchir et al. (2016) [47] compared t-z curve models from pressurimeter test results and analyzed their stiffness, proposing considerations for pile settlement calculations. Grecu et al. (2019) [48] introduced static t-z curves for suction caissons in marine sand, suggesting implementation in preliminary foundation design.

The importance of load transfer curves in analyzing pile behavior under axial and lateral loads has grown significantly, leading to improved predictive capabilities. In India, load settlement behavior is primarily assessed through field tests, with limited consideration given to theoretical load settlement curves. Theoretical curves are essential, particularly in situations where field tests are impractical, necessitating reliance on static pile load formulas. Thus, there arises a necessity for theoretical load settlement curves in India, in addition to improving codal provisions.

Considering these requirements, an attempt is made to perform a comparative study of the applicability of load transfer theories proposed by various scientists and predicting pile behavior based on them. This study aims to refine pile foundation design accuracy by comparing various load transfer theories and aligning numerical predictions with field test results. Objectives include enhancing design reliability, investigating new construction materials and techniques, and broadening parameters for future research.

## II. METHODOLOGY

The framework of the study, as illustrated in Figure 1, follows a systematic process to develop a composite curve based on different soil types. The study commenced with an extensive literature review in the relevant field. Based on the review, suitable studies were selected, with six studies being chosen for further analysis. Each of these studies provided two equations for calculating the load transfer curve, describing the pile-soil interaction along both the shaft and tip of the pile. Using these equations, load-settlement curves were generated. Next, a code was developed to estimate the relationship between load and settlement for various pile dimensions and soil types using octave software. For each soil type and pile configuration, a specific code was formulated to address variations in load behavior. The optimum load for each scenario was then determined using the allowable bearing load formula as per the Indian Standard code. To enhance the analysis, weightage of each study is evaluated by using best worst method (BWM) for each type of soil based on the calculated allowable load. Finally, based on these weighted curves, a composite curve was developed for different soil types. This composite curve streamlines load calculation by integrating the effects of soil type and pile dimensions, providing an accurate and efficient method for determining load capacities.

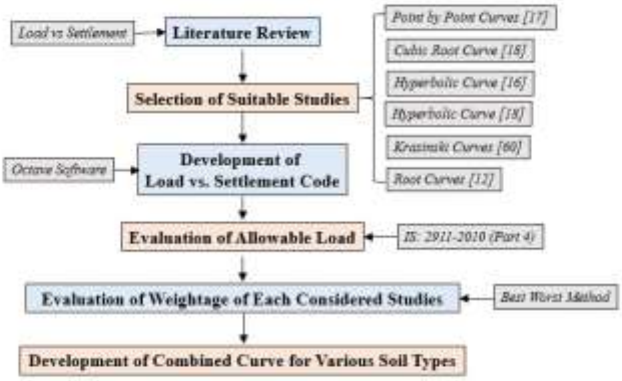


**Fig. 1.** Framework of the study

### A. OCTAVE Software

In this study, octave software is used for developing the code for load vs settlement curve. Octave is a high-level language, primarily intended for numerical computations [49]. It provides a convenient command line interface for solving linear and nonlinear problems numerically, and for performing other numerical experiments using a language that is mostly compatible with Matlab. It may also be used as a batch-oriented language. Octave has extensive tools for solving common numerical linear algebra problems, finding the roots of nonlinear equations, integrating ordinary functions, manipulating polynomials, and integrating ordinary differential and differential-algebraic equations. It is easily extensible and customizable via user-defined functions written in Octave's own language, or using dynamically loaded modules written in C++, C, Fortran, or other languages. Octave is also freely redistributable software. We may redistribute it and/or modify it under the terms of the GNU General Public License (GPL) as published by the Free Software Foundation.

### B. Data Analysis and Decision Tree

The investigation delved into determining the most precise methodology for specific soil and pile conditions using a decision tree model implemented in Python. A decision tree, akin to a flowchart, employs internal nodes to represent features or attributes, branches to depict decision rules, and leaf nodes to signify outcomes. The root node, situated at the top, initiates the partitioning process based on attribute values, recursively dividing the tree. This structured visualization aids decision-making by mirroring human thought processes, rendering decision trees comprehensible and interpretable. Notably, decision trees are transparent algorithms, sharing their internal decision-making logic, unlike opaque models such as Neural Networks, resulting in expedited training times. The computational complexity of decision trees hinges on the dataset's size and attribute count. Being distribution-free, decision trees do not rely on probability distribution assumptions, thus accommodating high-dimensional data with notable accuracy. The fundamental principle underlying any decision tree algorithm involves selecting the optimal attribute via Attribute Selection Measures (ASM) to split the dataset, subsequently forming decision nodes and iteratively partitioning the data into smaller subsets until certain termination conditions are met, such as complete attribute homogeneity or exhaustion of attributes or instances.

The investigation delved into determining the most precise methodology for specific soil and pile conditions using a decision tree model implemented in Python. A decision tree, akin to a flowchart, employs internal nodes to represent features or attributes, branches to depict decision rules, and leaf nodes to signify outcomes. The root node, situated at the top, initiates the partitioning process based on attribute values, recursively dividing the tree. This structured visualization aids decision-making by mirroring human thought processes, rendering decision trees comprehensible and interpretable. Notably, decision trees are transparent algorithms, sharing their internal decision-making logic, unlike opaque models such as Neural Networks, resulting in expedited training times. The computational complexity of decision trees hinges on the dataset's size and attribute count. Being distribution-free, decision trees do not rely on probability distribution assumptions, thus accommodating high-dimensional data with notable accuracy. The fundamental principle underlying any decision tree algorithm involves selecting the optimal attribute via Attribute Selection Measures (ASM) to split the dataset, subsequently forming decision nodes and iteratively partitioning the data into smaller subsets until certain termination conditions are met, such as complete attribute homogeneity or exhaustion of attributes or instances.

### *C. Best Worst Method*

A variety of Multi-Criteria Decision-Making (MCDM) methods are available to support decision-making processes, including the Aggregated Indices Randomization Method (AIRM), Analytic Hierarchy Process (AHP), Analytic Network Process (ANP), Fuzzy AHP, Base-Criterion Method (BCM), and Best-Worst Method (BWM), among others. Among these, BWM, introduced by Prof. Rezaei [50], stands out as an exceptional tool. It requires fewer pairwise comparisons than other methods, leading to more efficient and reliable results while significantly reducing the time needed for analysis. Due to these advantages, BWM has been chosen for this study. This method has been widely applied across various fields. The procedure for implementing this method is outlined below:

***Step* 1**: The decision criteria for achieving the ultimate objective of the study can be defined as $\{o_1, o_2, o_3 \ldots\ldots o_n\}$, where each o represents a specific criterion associated with the objective.

***Step* 2**: The decision-maker must identify the best (i.e., most significant) and the worst (i.e., least significant) criteria among all the options.

***Step* 3:** The preference of the best criterion over the other criteria should be assessed using a scale from 1 to 9, where 1 signifies equal preference, and 9 indicates a strong preference. The preferences can be represented as follows:

$$A_B = (a_{b1}, a_{b2}, a_{b3} \ldots\ldots, a_{bn})$$

***Step* 4:** Similarly, the preference of the worst criterion over the other criteria should be evaluated using a scale from 1 to 9, where 1 represents equal preference and 9 signifies strong preference.

$$A_W = (a_{w1}, a_{w2}, a_{w3} \ldots\ldots, a_{wn})$$

***Step* 5:** In this step, optimal weights ( $w_1^*, w_2^*, w_3^* \ldots\ldots, w_n^*$ ) for each criterion are calculated by ensuring that the conditions $w_B/w_j$ and $w_j/w_W$. The best possible solution is $w_B/w_j = a_{Bj}$ and $w_j/w_W = a_{jw}$. To obtain these two solutions, maximum among the set of $\{|w_B - w_j \times a_{Bj}|$ and $|w_j - w_W \times a_{jw}|\}$ should be minimized as follows:

$$\text{Min, } \max_j\{|w_B - w_j \times a_{Bj}| \text{ and } |w_j - w_W \times a_{jw}|\}$$

Subjected to

$$\sum_j w_j = 1,\ w_j \geq 0 \text{ for all } j \qquad \ldots\ldots\ldots\ldots\ldots\text{(i)}$$

The equation (i) can be converted into a linear problem as follows:

$$\min,\ \xi^L$$

$$\sum_j w_j = 1$$

Subjected to,

$$|w_B - a_{Bj}\, w_j| \leq \xi^L \text{ for all j}$$

$$|w_j - a_{jw}\, w_W| \leq \xi^L \text{ for all j}$$

$$\sum_j w_j = 1,\ w_j \geq 0 \text{ for all } j \qquad \ldots\ldots\ldots\ldots\ldots\text{(ii)}$$

By using the linear problem, the optimal weights of each criterion and $\xi^{L^*}$ can be evaluated.

## III. Experimental Results

### *A. Load vs Settlement*

The details of typical lengths and capacities of various pile types are shown in Annexure I [51-53]. This information is used only as a guideline in the initial planning and analysis stages. For this study the various parameters of the soil such as bearing capacity factor (Nq), earth pressure coefficient (K), internal friction angle (Ø), unit weight (ɣ) and pile soil friction angle (δ), were obtained by taking reference of Indian Standard Code 2911 (Part 1) as shown in Tables II and III [54-57]. The pile material used is concrete pile. The analysis of the study is applicable only for driven piles. The value of δ for driven pile is obtained from Indian Standard Code 2911. Five different diameter (B) and length

(L) of concrete piles were considered for the analysis as shown in Table IV [58-60].

VALUES OF K (EARTH PRESSURE COEFFICIENT) AND Δ

| Pile material | Δ | K for loose sand | K for dense sand |
|---|---|---|---|
| Concrete | 0.75Ø | 1.0 | 2.0 |

THE DIFFERENT SOIL PARAMETERS AND THEIR SOURCES WHICH WERE USED FOR DRIVEN PILES

| Type of sand | Nq | K | Ø | ɣ | δ |
|---|---|---|---|---|---|
| **Silty sand** | 58 | 1.2 | 35 | 18 | 30 |
| **Loose sand** | 17 | 1 | 32 | 16.40 | 18.8 |
| **Uniform sand** | 60 | 1.3 | 35 | 17.3 | 26.3 |
| **Medium sand** | 22 | 1 | 27 | 18 | 20.25 |
| **Dense sand** | 137 | 2 | 40 | 18 | 30 |
| **Fine sand** | 68 | 1 | 36 | 17.3 | 27 |

DIMENSION OF PILE

| Sl. No. | Diameter in m (B) | Length in m (L) |
|---|---|---|
| 1 | 0.5 | 12 |
| 2 | 0.2 | 8 |
| 3 | 0.25 | 12 |
| 4 | 0.45 | 20 |
| 5 | 0.45 | 9 |

In this analysis, total 6 number of studies related to load transfer curves are selected as shown in Table V. Additionally, 6 types of soil conditions are considered such as uniform sand, loose sand, medium sand, dense sand, fine sand, and silty sand soil.

SELECTED STUDIES OF THE ANALYSIS

| Study | Name of the curve | Mathematical expression | Reference |
|---|---|---|---|
| 1 | Point by point curves | **Shaft**<br>***For Clay***<br>$S_s/D$ — $q_s/q_{s,ult}$<br>0,0016 — 0,30<br>0,0031 — 0,50<br>0,0057 — 0,75<br>0,0080 — 0,90<br>0,0100 — 1,00<br>0,0200 — 0,70 to 0,90<br>Infinity — 0,70 to 0,90<br>***For Sand***<br>$S_s$ (mm) — $q_s/q_{s,ult}$<br>0,00 — 0,00<br>2,54 — 1,00<br>Infinity — 1,00<br>**Tip**<br>$S_b/B$ — $q_b/q_{b,ult}$<br>0,002 — 0,25<br>0,013 — 0,50<br>0,042 — 0,75<br>0,073 — 0,90<br>0,100 — 1,00 | [17] |
| 2 | Cubic root curve | $Shaft: q_s = \min\left\{\begin{matrix} (\frac{S_s}{S_{s,ult}})^{1/3} q_{s,ult} \\ q_{s,ult} \end{matrix}\right\}$<br>$Tip: q_b = \min\left\{\begin{matrix} (\frac{S_b}{S_{b,\lim}})^{1/3} q_{b,ult} \\ q_{b,ult} \end{matrix}\right\}$ | [18] |
| 3 | Hyperbolic Curve | $Shaft: q_s = \frac{q_{s,ult} S_s}{0.0025B + S_s}$<br>$Tip: q_b = \frac{q_{b,ult} S_b}{0.25B + S_b}$ | [16] |
| 4 | Hyperbolic Curve | $Shaft: q_s = \frac{q_{s,ult} S_s}{MB + S_s}$<br>$Tip: q_b = \frac{q_{b,ult} S_b}{0.6\pi \frac{B}{4E} q_{b,ult} + S_b}$ | [18] |
| 5 | Krasinski | $Shaft: q_s = \min\left\{\begin{matrix} q_{s,ult} (\frac{S_s}{S_{s,\lim}})^{.038} \\ q_{s,ult} \end{matrix}\right\}$<br>$Tip: q_b = \min\left\{\begin{matrix} q_{b,ult} (\frac{S_b}{S_{b,\lim}})^{0.38} \\ q_{b,ult} \end{matrix}\right\}$ | [61] |
| 6 | Root curve | $Shaft: q_s = \min\left\{\begin{matrix} (2\sqrt{\frac{S_s}{S_{s,\lim}}} - \frac{S_s}{S_{s,\lim}}) q_{s,ult} \\ q_{s,ult} \end{matrix}\right\}$<br>$Tip: q_b = \min\left\{\begin{matrix} (\frac{S_b}{S_{b,\lim}})^{1/3} q_{b,ult} \\ q_{b,ult} \end{matrix}\right\}$ | [12] |

These load transfer curves were considered since the other load transfer curves required some additional values such as pressure-meter modulus, shear modulus, radius of influence, poissons' ratio which are difficult to obtain at times. The load transfer curves that were considered had minimum requirements and were very convenient to use. Moreover the probable extensions of their domain of validity were studied by applying these curves to soil types which were not suggested by their founders. The results suggested that the curves can be used outside their domain. After selection of 5 classes for pile dimensions and 6 types of soil conditions, load vs settlement codes are developed using octave software. Here under each type of soil there are 5 classes of pile dimensions, and under each class of pile dimension there are 6 studies which gives equations for load vs settlement curve. So, in this study, total 180 load vs settlement curves are developed. A sample code of Point by point curves for dense sandy soil, length 8m and diameter 0.2m is given in Annexure II.

## B. Allowable Load Calculations

According to IS: 2911-2010 (Part 4), the allowable load may be taken using the following equation (iii).

$$\text{Allowable load} = \begin{Bmatrix} \frac{2}{3} \times \text{Final load at 12mm settlement} \\ \frac{1}{2} \times \text{Load at a point where settlement value is 10\% of pile diameter} \end{Bmatrix}_{\min} \quad \text{.........(iii)}$$

So, after the development of 180-load vs settlement curves, the loads at 12 mm settlement and loads required to give settlement, which is equal to 10% of pile diameter, are extracted for each curve. Using the extracted information from each curve, the allowable load for driven piles for various cases (various pile types, pile dimensions and considered studies) is calculated. The evaluated allowable load for various cases are shown in Table VI.

ALLOWABLE LOAD FOR VARIOUS CASES

| Study | Studies | Load at 12mm settlement | Load at 10% pile diameter settlement | Allowable load |
|---|---|---|---|---|
| | ***For Silty sand, B = 0.5m and L = 12m*** | | | |
| S1 | Point by point curves | 2654.30 | 3397.30 | 1698.65 |
| S2 | Cubic root curve | 2184.20 | 3587.80 | 1456.13 |
| S3 | Hirayama curve | 1323.30 | 2187.60 | 882.20 |
| S4 | Hyperbolic curve | 2431.30 | 3587.80 | 1620.87 |
| S5 | Krasinski | 2095.90 | 3496.20 | 1397.27 |
| S6 | Root curve | 2129.80 | 3004.40 | 1419.87 |
| | ***For Loose sand, B = 0.5m and L = 12m*** | | | |
| S1 | Point by point curves | 669.85 | 817.40 | 408.69 |
| S2 | Cubic root curve | 692.10 | 817.40 | 408.69 |
| S3 | Hirayama curve | 415.22 | 817.40 | 276.81 |
| S4 | Hyperbolic curve | 679.65 | 817.40 | 408.69 |
| S5 | Krasinski | 585.17 | 817.40 | 390.12 |
| S6 | Root curve | 2157.20 | 3199.10 | 1438.13 |
| | ***For Uniform sand, B = 0.5m and L = 12m*** | | | |
| S1 | Point by point curves | 2757.9 | 3736.6 | 1836.6 |
| S2 | Cubic root curve | 2267.1 | 3736.6 | 1511.4 |
| S3 | Hirayama curve | 1471.1 | 3736.6 | 985.73 |
| S4 | Hyperbolic curve | 2526.9 | 3736.6 | 1684.6 |
| S5 | Krasinski | 2181.6 | 3736.6 | 1454.4 |
| S6 | Root curve | 2157.2 | 3199.1 | 1438.13 |
| | ***For Medium sand, B = 0.5m and L = 12m*** | | | |
| S1 | Point by point curves | 1314 | 1528.1 | 876 |
| S2 | Cubic root curve | 1292.7 | 1601.3 | 861.8 |
| S3 | Hirayama curve | 2666.3 | 1601.3 | 1067.53 |
| S4 | Hyperbolic curve | 1270.3 | 1601.3 | 846.87 |
| S5 | Krasinski | 1087.8 | 1586.9 | 725.2 |
| S6 | Root curve | 1153.3 | 1367.9 | 768.87 |
| | ***For Dense sand, B = 0.5m and L = 12m*** | | | |
| S1 | Point by point curves | 2937.7 | 7374.6 | 1958.47 |
| S2 | Cubic root curve | 2217.5 | 7903.1 | 1478.3 |
| S3 | Hirayama curve | 2440 | 7903.1 | 1626.67 |
| S4 | Hyperbolic curve | 3182.7 | 7903.1 | 2121.8 |
| S5 | Krasinski | 2095.4 | 7166.3 | 1396.93 |
| S6 | Root curve | 2188.1 | 6449.9 | 1458.73 |
| | ***For Fine sand, B = 0.5m and L = 12m*** | | | |
| S1 | Point by point curves | 2550.3 | 3442 | 1700.2 |
| S2 | Cubic root curve | 2004 | 3659.5 | 1336 |
| S3 | Hirayama curve | 1091.9 | 3659.5 | 727.93 |
| S4 | Hyperbolic curve | 2353.6 | 3659.5 | 1569.07 |
| S5 | Krasinski | 2008.1 | 3616.8 | 1338.73 |
| S6 | Root curve | 1986.5 | 3050.4 | 1324.33 |
| | ***For Medium sand, B = 0.2m and L = 8m*** | | | |
| S1 | Point by point curves | 170.27 | 172.90 | 86.45 |
| S2 | Cubic root curve | 175.16 | 176.59 | 88.30 |
| S3 | Hirayama curve | 176.59 | 176.59 | 88.30 |
| S4 | Hyperbolic curve | 168.93 | 176.59 | 88.30 |
| S5 | Krasinski | 153.13 | 176.59 | 88.30 |
| S6 | Root curve | 163.07 | 164.14 | 82.07 |
| | ***Fine sand, B = 0.2m and L = 8m*** | | | |
| S1 | Point by point curves | 263.07 | 271.4 | 135.7 |
| S2 | Cubic root curve | 274.75 | 283.47 | 141.74 |
| S3 | Hirayama curve | 175.73 | 283.47 | 117.15 |
| S4 | Hyperbolic curve | 258.82 | 283.47 | 141.74 |
| S5 | Krasinski | 231.53 | 277.67 | 138.84 |
| S6 | Root curve | 240.44 | 250.99 | 125.50 |
| | ***Dense sand, B = 0.2m and L = 8m*** | | | |
| S1 | Point by point curves | 400.21 | 425.22 | 212.61 |
| S2 | Cubic root curve | 412.69 | 451.88 | 225.94 |
| S3 | Hirayama curve | 193.54 | 451.88 | 129.03 |
| S4 | Hyperbolic curve | 389.88 | 451.88 | 225.94 |
| S5 | Krasinski | 333.84 | 426.67 | 213.34 |
| S6 | Root curve | 353.12 | 374.38 | 187.19 |
| | ***Loose sand, B = 0.2m and L = 8m*** | | | |
| S1 | Point by point curves | 118.98 | 114.48 | 82.86 |
| S2 | Cubic root curve | 168.94 | 170.95 | 85.47 |
| S3 | Hirayama curve | 170.95 | 170.95 | 85.47 |
| S4 | Hyperbolic curve | 160.11 | 170.95 | 85.47 |
| S5 | Krasinski | 146.11 | 170.95 | 85.47 |
| S6 | Root curve | 184.51 | 186.98 | 93.49 |
| | ***Uniform sand, B = 0.2m and L = 8m*** | | | |
| S1 | Point by point curves | 653.02 | 697.7 | 348.85 |
| S2 | Cubic root curve | 553.03 | 735.43 | 367.72 |
| S3 | Hirayama curve | 406.67 | 735.43 | 272.46 |
| S4 | Hyperbolic curve | 631.59 | 735.43 | 367.72 |
| S5 | Krasinski | 514.28 | 694.89 | 344.56 |
| S6 | Root curve | 500.38 | 649.44 | 324.72 |
| | ***Silty sand, B = 0.2m and L = 8m*** | | | |
| S1 | Point by point curves | 634.97 | 669.53 | 354.41 |
| S2 | Cubic root curve | 525.87 | 707.82 | 353.91 |
| S3 | Hirayama curve | 390.33 | 707.82 | 260.22 |
| S4 | Hyperbolic curve | 521.35 | 707.82 | 304.24 |
| S5 | Krasinski | 521.83 | 656.17 | 347.89 |
| S6 | Root curve | 520.88 | 614.48 | 307.24 |
| | ***Loose sand, B = 0.45m and L = 9m*** | | | |
| S1 | Point by point curves | 1519.3 | 4892.9 | 1017.93 |
| S2 | Cubic root curve | 518.89 | 611.24 | 305.62 |
| S3 | Hirayama curve | 292.29 | 611.24 | 195.83 |
| S4 | Hyperbolic curve | 1840.9 | 6490.2 | 1233.4 |
| S5 | Krasinski | 450.81 | 608.21 | 302.04 |
| S6 | Root curve | 579.04 | 692.39 | 346.19 |
| | ***Medium sand, B = 0.45m and L = 9m*** | | | |
| S1 | Point by point curves | 1032.4 | 1148.5 | 574.25 |
| S2 | Cubic root curve | 1027.8 | 1206.9 | 603.45 |
| S3 | Hirayama curve | 523.67 | 1206.9 | 350.85 |
| S4 | Hyperbolic curve | 1000.7 | 1206.9 | 603.45 |
| S5 | Krasinski | 876.01 | 1193.9 | 586.92 |
| S6 | Root curve | 883.54 | 1017.9 | 508.95 |
| | ***Fine sand, B = 0.45m and L = 9m*** | | | |
| S1 | Point by point curves | 2081.7 | 2654.7 | 1387.8 |
| S2 | Cubic root curve | 2057.6 | 2844.5 | 1371.73 |
| S3 | Hirayama curve | 798.45 | 2844.5 | 532.3 |
| S4 | Hyperbolic curve | 2035.9 | 2844.5 | 1357.27 |
| S5 | Krasinski | 1659.8 | 2725.6 | 1106.53 |
| S6 | Root curve | 1766.9 | 2351.1 | 1175.6 |
| | ***Silty sand, B = 0.45m and L = 9m*** | | | |

| | | | | |
|---|---|---|---|---|
| S1 | Point by point curves | 1048.20 | 1177.90 | 588.95 |
| S2 | Cubic root curve | 1035.00 | 1228.20 | 614.10 |
| S3 | Hirayama curve | 6519.00 | 1228.20 | 614.10 |
| S4 | Hyperbolic curve | 1018.20 | 1228.20 | 614.10 |
| S5 | Krasinski | 8508.70 | 1204.60 | 602.30 |
| S6 | Root curve | 9003.10 | 1045.20 | 522.60 |
| | ***Uniform sand, B = 0.45m and L = 9m*** | | | |
| S1 | Point by point curves | 842.63 | 954.49 | 477.25 |
| S2 | Cubic root curve | 834.64 | 1005.50 | 502.75 |
| S3 | Hirayama curve | 408.59 | 1005.50 | 272.39 |
| S4 | Hyperbolic curve | 813.74 | 1005.50 | 502.75 |
| S5 | Krasinski | 969.20 | 994.21 | 497.11 |
| S6 | Root curve | 727.07 | 860.42 | 430.21 |
| | ***Dense sand, B = 0.45m and L = 9m*** | | | |
| S1 | Point by point curves | 1480.10 | 1801.9 | 900.95 |
| S2 | Cubic root curve | 1447.30 | 1928.5 | 964.87 |
| S3 | Hirayama curve | 490.90 | 1928.5 | 327.27 |
| S4 | Hyperbolic curve | 1405.40 | 1928.5 | 936.93 |
| S5 | Krasinski | 1200.30 | 1874.0 | 800.20 |
| S6 | Root curve | 1204.40 | 1536.2 | 768.10 |
| | ***Loose sand, B = 0.45m and L = 20m*** | | | |
| S1 | Point by point curves | 1063.3 | 2262.2 | 712.41 |
| S2 | Cubic root curve | 812.47 | 921.95 | 460.97 |
| S3 | Hirayama curve | 596.65 | 921.95 | 399.75 |
| S4 | Hyperbolic curve | 1032.6 | 2956.2 | 691.84 |
| S5 | Krasinski | 667.23 | 909.54 | 447.04 |
| S6 | Root curve | 868.73 | 1003.1 | 501.55 |
| | ***Medium sand, B = 0.45m and L = 20m*** | | | |
| S1 | Point by point curves | 1474.3 | 1692.4 | 846.2 |
| S2 | Cubic root curve | 1136.6 | 1757.9 | 761.52 |
| S3 | Hirayama curve | 1052 | 1757.9 | 704.84 |
| S4 | Hyperbolic curve | 1276.6 | 1757.9 | 855.32 |
| S5 | Krasinski | 1097.6 | 1706.2 | 735.39 |
| S6 | Root curve | 1109 | 1568.8 | 743.03 |
| | ***Fine sand, B = 0.45m and L = 20m*** | | | |
| S1 | Point by point curves | 1629.7 | 3327.8 | 1091.7 |
| S2 | Cubic root curve | 1145.3 | 3575.9 | 767.35 |
| S3 | Hirayama curve | 1383.2 | 3575.9 | 922.13 |
| S4 | Hyperbolic curve | 1721.4 | 3575.9 | 1147.6 |
| S5 | Krasinski | 1139.4 | 3230.5 | 759.6 |
| S6 | Root curve | 1114.7 | 3082.5 | 743.13 |
| | ***Silty sand, B = 0.45m and L = 20m*** | | | |
| S1 | Point by point curves | 1714 | 3556.2 | 1142.47 |
| S2 | Cubic root curve | 1109 | 3771.5 | 739.33 |
| S3 | Hirayama curve | 1671.7 | 2637.4 | 1114.47 |
| S4 | Hyperbolic curve | 1858.9 | 3771.5 | 1239.27 |
| S5 | Krasinski | 1160.1 | 3480.8 | 773.4 |
| S6 | Root curve | 1093.5 | 3298.9 | 729 |
| | ***Uniform sand, B = 0.45m and L = 20m*** | | | |
| S1 | Point by point curves | 1746 | 3690.8 | 1164 |
| S2 | Cubic root curve | 1040.5 | 3075.7 | 693.67 |
| S3 | Hirayama curve | 739.3 | 3916.6 | 492.87 |
| S4 | Hyperbolic curve | 1860.9 | 3632.6 | 1240.6 |
| S5 | Krasinski | 2300.6 | 3589.7 | 1533.73 |
| S6 | Root curve | 2192.4 | 3481.3 | 1461.6 |
| | ***Dense sand, B = 0.45m and L = 20m*** | | | |
| S1 | Point by point curves | 1490 | 4973.9 | 993.6 |
| S2 | Cubic root curve | 1044.9 | 3055.5 | 696.60 |
| S3 | Hirayama curve | 2372.9 | 4908.4 | 1581.93 |
| S4 | Hyperbolic curve | 17779.6 | 5748.6 | 11853.067 |
| S5 | Krasinski | 1039.3 | 3715.2 | 692.87 |
| S6 | Root curve | 992.9 | 3192.3 | 661.93 |
| | ***Loose sand, B = 0.25m and L = 12m*** | | | |
| S1 | Point by point curves | 491.99 | 882.45 | 329.63 |
| S2 | Cubic root curve | 284.57 | 298.5 | 149.25 |
| S3 | Hirayama curve | 207.69 | 298.5 | 139.15 |
| S4 | Hyperbolic curve | 450.12 | 904.84 | 301.58 |
| S5 | Krasinski | 241.13 | 295.06 | 147.53 |
| S6 | Root curve | 306.44 | 323.54 | 161.77 |
| | ***Medium sand, B = 0.25m and L = 12m*** | | | |
| S1 | Point by point curves | 520.61 | 546.99 | 273.49 |
| S2 | Cubic root curve | 523.16 | 567.28 | 283.64 |
| S3 | Hirayama curve | 366.11 | 567.28 | 245.29 |
| S4 | Hyperbolic curve | 511.72 | 567.28 | 283.64 |
| S5 | Krasinski | 440.03 | 552.32 | 276.16 |
| S6 | Root curve | 476.05 | 508.94 | 254.47 |
| | ***Silty sand, B = 0.25m and L = 12m*** | | | |
| S1 | Point by point curves | 794.06 | 1141.9 | 264.69 |
| S2 | Cubic root curve | 546.71 | 1058.5 | 182.24 |
| S3 | Hirayama curve | 652.10 | 860.46 | 217.4 |
| S4 | Hyperbolic curve | 879.64 | 1126.2 | 293.21 |
| S5 | Krasinski | 551.64 | 1107.6 | 183.88 |
| S6 | Root curve | 580.5 | 1064.6 | 193.50 |
| | ***Uniform sand, B = 0.25m and L = 12m*** | | | |
| S1 | Point by point curves | 812.32 | 1184.6 | 541.55 |
| S2 | Cubic root curve | 599.55 | 1076.1 | 399.7 |
| S3 | Hirayama curve | 1530.5 | 1724.5 | 862.25 |
| S4 | Hyperbolic curve | 886.77 | 1163.9 | 581.95 |
| S5 | Krasinski | 565.45 | 1148.7 | 376.97 |
| S6 | Root curve | 557.15 | 1122.3 | 371.43 |
| | ***Fine sand, B = 0.25m and L = 12m*** | | | |
| S1 | Point by point curves | 827.56 | 1054.9 | 527.45 |
| S2 | Cubic root curve | 560.1 | 1058.8 | 373.4 |
| S3 | Hirayama curve | 521.92 | 1136.5 | 347.95 |
| S4 | Hyperbolic curve | 839.58 | 1036.9 | 518.45 |
| S5 | Krasinski | 574.27 | 1017.1 | 382.85 |
| S6 | Root curve | 568.507 | 984.22 | 379.00 |
| | ***Dense sand, B = 0.25m and L = 12m*** | | | |
| S1 | Point by point curves | 925.88 | 1491.9 | 617.3 |
| S2 | Cubic root curve | 523.67 | 1104.4 | 349.1 |
| S3 | Hirayama curve | 1040.7 | 1559.2 | 693.8 |
| S4 | Hyperbolic curve | 932.72 | 1651.7 | 621.8 |
| S5 | Krasinski | 588.17 | 1098.5 | 392.1 |
| S6 | Root curve | 576.56 | 1119.1 | 384.4 |

The table provides a comparison of loads at different settlement levels for various types of sands (silty, loose, uniform, medium, fine, and dense) under different conditions of B and L. The loads are compared across different studies represented by various curve such as point by point curves, cubic root curve, Hirayama curve, hyperbolic curve, Krasinski, and root curve. The loads vary significantly across different settlement levels, indicating the sensitivity of the soil to applied loads. For example, at 12mm settlement, the loads are generally lower compared to the loads at 10% pile diameter settlement. Different types of sands exhibit distinct load-bearing capacities. For instance, dense sand generally has higher load-bearing capacities compared to loose or fine sand. This aligns with the expected behavior, as denser sands typically offer better support due to their compactness. The dimensions of the B and L also play a crucial role in determining the load-bearing capacity. For example, when comparing the same type of sand with different base dimensions, it can be observed variations in load-bearing capacities. A larger diameter or length generally results in higher load-bearing capacities. Different curve yield slightly different results. For instance, while the point by point curves and hyperbolic curve may provide similar results for some soil types, there could be variations in others. This indicates the importance of selecting an appropriate curve technique based on the specific soil characteristics and project requirements. The reliability and accuracy of the results depend on various factors such as the quality of data, appropriateness of the curve technique, and representativeness of the soil samples. Engineers and researchers need to consider these factors while interpreting and utilizing the results for practical applications. The table's data can be valuable for geotechnical engineers, foundation designers, and construction professionals involved in designing and analyzing pile foundations. It helps them understand the expected behavior of different types of sands under varying conditions and make informed decisions during the design process.

### C. Assigning of Weightage

In this study, the Best-Worst Method (BWM) is utilized to assign weights to six load vs settlement studies based on their corresponding values. This approach ensures that methods with higher values, which represent better performance or greater preference, receive higher weights, while maintaining that the total weight sum equals 1 []. The provided values for each method serve as the basis for calculating their relative importance. For silty sand (B = 0.5m and L = 12m), it is observed that Study 3 yields the lowest allowable load, whereas Study 1 provides the highest allowable load. A lower allowable load indicates that the structure will bear a minimal load on that soil, making the design inherently safer. Conversely, a higher allowable load implies a higher risk, as the soil would be subjected to its maximum capacity. Thus, a study offering the minimum allowable load is considered the best for that soil type, while a study yielding the maximum allowable load is deemed the least favorable. The preference of the best and worst criterion over the other criteria for silty soil (B=0.5m and L=12m) is shown in Annexure III. By evaluating the allowable loads across various soil conditions and studies, the weight of each study has been calculated for different soil types with varying dimensions, as detailed in Table VII.

WEIGHTAGE OF EACH STUDY FOR VARIOUS SOIL TYPES AND DIMENSIONS

| Soil Type | S1 | S2 | S3 | S4 | S5 | S6 |
|---|---|---|---|---|---|---|
| ***B = 0.5m and L = 12m*** | | | | | | |
| Silty Sand | 0.0519 | 0.1038 | 0.4672 | 0.0742 | 0.1731 | 0.1298 |
| Loose sand | 0.1666 | 0.1666 | 0.2751 | 0.1866 | 0.1639 | 0.0412 |
| Uniform sand | 0.1095 | 0.1522 | 0.2111 | 0.1488 | 0.1798 | 0.1986 |
| Medium sand | 0.1534 | 0.1654 | 0.1244 | 0.1777 | 0.1966 | 0.1825 |
| Danse Sand | 0.1134 | 0.1832 | 0.1633 | 0.1792 | 0.1932 | 0.1677 |
| Fine Sand | 0.1211 | 0.1624 | 0.1942 | 0.1788 | 0.1833 | 0.1602 |
| ***B = 0.2m and L = 8m*** | | | | | | |
| Silty Sand | 0.1276 | 0.1467 | 0.2022 | 0.1622 | 0.1833 | 0.178 |
| Loose sand | 0.1211 | 0.1624 | 0.1942 | 0.1788 | 0.1833 | 0.1602 |
| Uniform sand | 0.1666 | 0.1666 | 0.2751 | 0.1866 | 0.1639 | 0.0412 |
| Medium sand | 0.1765 | 0.1592 | 0.1592 | 0.1592 | 0.1592 | 0.1867 |
| Danse Sand | 0.1211 | 0.1624 | 0.1942 | 0.1788 | 0.1833 | 0.1602 |
| Fine Sand | 0.1642 | 0.1287 | 0.2112 | 0.1287 | 0.1763 | 0.1909 |
| ***B = 0.45m and L = 9m*** | | | | | | |
| Silty Sand | 0.2098 | 0.1298 | 0.1298 | 0.1298 | 0.1654 | 0.2354 |
| Loose sand | 0.1134 | 0.1832 | 0.1633 | 0.1792 | 0.1932 | 0.1677 |
| Uniform sand | 0.1276 | 0.1467 | 0.2022 | 0.1622 | 0.1833 | 0.178 |
| Medium sand | 0.1211 | 0.1624 | 0.1942 | 0.1788 | 0.1833 | 0.1602 |
| Danse Sand | 0.1134 | 0.1832 | 0.1633 | 0.1792 | 0.1932 | 0.1677 |
| Fine Sand | 0.1498 | 0.1721 | 0.1693 | 0.1244 | 0.1834 | 0.201 |
| ***B = 0.45m and L = 20m*** | | | | | | |
| Silty Sand | 0.1211 | 0.1624 | 0.1942 | 0.1788 | 0.1833 | 0.1602 |
| Loose sand | 0.1666 | 0.1666 | 0.2751 | 0.1866 | 0.1639 | 0.0412 |
| Uniform sand | 0.2098 | 0.1298 | 0.1298 | 0.1298 | 0.1654 | 0.2354 |
| Medium sand | 0.1134 | 0.1832 | 0.1633 | 0.1792 | 0.1932 | 0.1677 |
| Danse Sand | 0.1534 | 0.1654 | 0.1244 | 0.1777 | 0.1966 | 0.1825 |
| Fine Sand | 0.1276 | 0.1467 | 0.2022 | 0.1622 | 0.1833 | 0.178 |
| ***B = 0.25m and L = 12m*** | | | | | | |
| Silty Sand | 0.1534 | 0.1654 | 0.1244 | 0.1777 | 0.1966 | 0.1825 |
| Loose sand | 0.1211 | 0.1624 | 0.1942 | 0.1788 | 0.1833 | 0.1602 |
| Uniform sand | 0.1666 | 0.1666 | 0.2751 | 0.1866 | 0.1639 | 0.0412 |
| Medium sand | 0.1276 | 0.1467 | 0.2022 | 0.1622 | 0.1833 | 0.178 |
| Danse Sand | 0.1211 | 0.1624 | 0.1942 | 0.1788 | 0.1833 | 0.1602 |
| Fine Sand | 0.1398 | 0.1822 | 0.2011 | 0.1578 | 0.1621 | 0.157 |

For silty sand, (B = 0.5), the Hirayama Curve has the highest weightage of 0.4672, followed by Root Curve (0.1298). The other curves such as Cubic Root and Point by Point also provide relevant results but with much lower weightages, indicating that for Silty Sand, the Hirayama method offers the most reliable model. As pile dimensions change to B = 0.2 and B = 0.45, the Hirayama Curve continues to dominate the weightage, though the Root Curve becomes more relevant with B = 0.45 (0.2354). Fine Sand shows the greatest variation, where the weightage for the Root Curve increases with larger pile dimensions, suggesting its higher adaptability under these conditions. In loose sand, there is a noticeable shift. For B = 0.5, the Cubic Root Curve and Hirayama Curve show relatively similar weightages, but Hirayama Curve seems to provide a better fit for B = 0.45, with 0.1721 for B = 0.45, L = 20. The Root Curve maintains a lower weightage, which shows that other methods like Cubic Root and Hirayama offer more robust solutions for modeling in Loose Sand.

For uniform sand (B = 0.5), the Cubic Root and Hirayama Curve show similar weightages, with Cubic Root slightly outperforming others. As the pile dimension decreases, especially for B = 0.25, the Cubic Root method becomes more useful, with weightages approaching 0.1666. The Point by Point method also performs well in this scenario, but not as strongly as others. In medium sand, the

Hyperbolic Curve generally performs well, with a stable weightage across different pile dimensions. B = 0.5 shows a 0.1777 weightage for this curve, while the Root Curve offers more consistent values, which can be beneficial for medium sand types across different pile dimensions. In dense sand, Hirayama Curve has a high weightage in this category, especially for B = 0.2 and B = 0.45, with values around 0.1833. This indicates that Hirayama might be a more accurate model for evaluating pile performance in dense sand, where particle structure and load distribution differ from looser sands. In fine sand, Hirayama and Root Curves emerge as the most relevant methods for Fine Sand, especially as pile dimensions increase. The Root Curve shows a significant rise in weightage with increasing pile dimension, indicating its advantage in predicting pile behavior under such conditions. The Hyperbolic Curve also shows a substantial weightage for B = 0.5, providing valuable insight for soil conditions with finer particles.

The Hirayama Curve is the most adaptable across various soil types, especially for Silty Sand and Dense Sand. Its high weightage in these categories suggests that it provides accurate predictions for a broad range of soil conditions and pile dimensions. The Root Curve, while not the top performer across all conditions, provides strong results in some specific scenarios, such as larger pile dimensions in Fine Sand and Silty Sand. The Point by Point and Cubic Root curves provide valuable contributions, particularly in Loose Sand and Uniform Sand conditions. They tend to be more consistent across the data set, though they sometimes fall behind other methods in accuracy. Larger pile dimensions (B = 0.45 and L = 20) generally result in better performance for the Root Curve and Hirayama Curve, while smaller pile dimensions (B = 0.2 and B = 8) tend to favor curves like Cubic Root and Point by Point. This suggests that pile dimension significantly affects the choice of curve for modeling pile behavior, as larger piles may require more complex models that account for deeper penetration and soil interaction. Silty Sand and Fine Sand benefit from the Hirayama Curve, while Loose Sand is more flexible with Cubic Root and Point by Point models. This indicates that understanding the soil type is crucial for selecting the most appropriate curve. For soils like Dense Sand, Medium Sand, and Uniform Sand, the Hyperbolic Curve and Root Curve offer more reliable predictions, indicating the need for these models in granular soils with different levels of compaction.

*D. Combination of the Curves*

After finding the weightage of each studies, the determined weightage was then used to determine the composite curve for a particular soil type. The composite curves are elucidated in the figure 2 (a-f). The composite curve presented here corresponds to various soil conditions for B = 0.5m and L = 12m. Similarly, curves for other dimensions can be combined in the same manner.

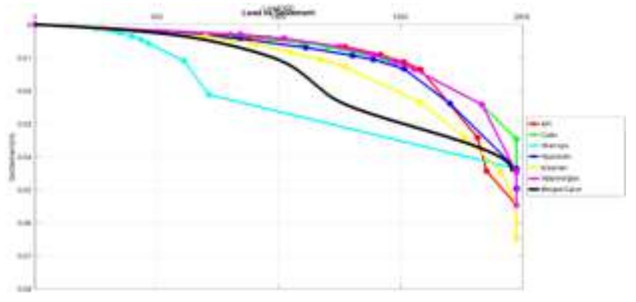

(a) Uniform Sand

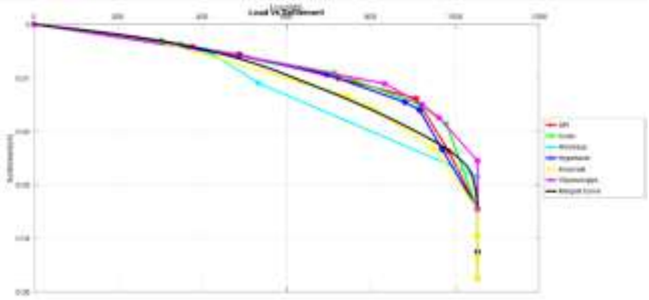

(b) Silty Sand

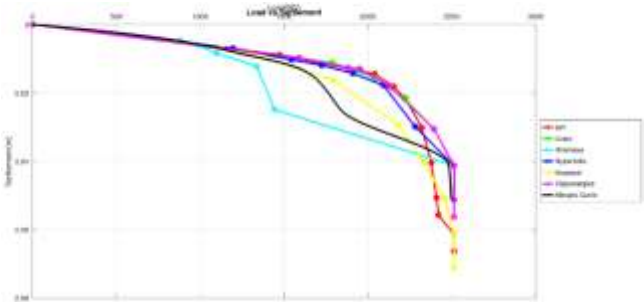

(c) Medium Sand

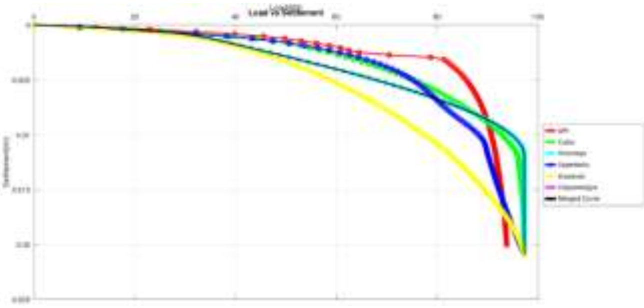

(d) Loose Sand

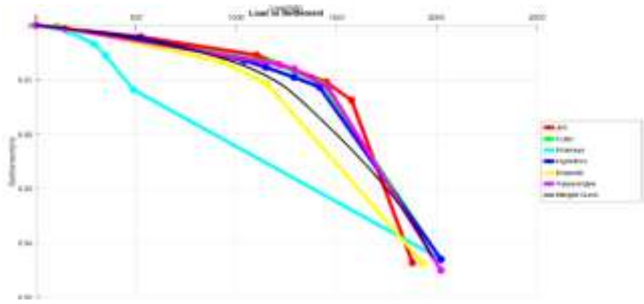

(e) Fine Sand

Identify applicable funding agency here. If none, delete this text box.

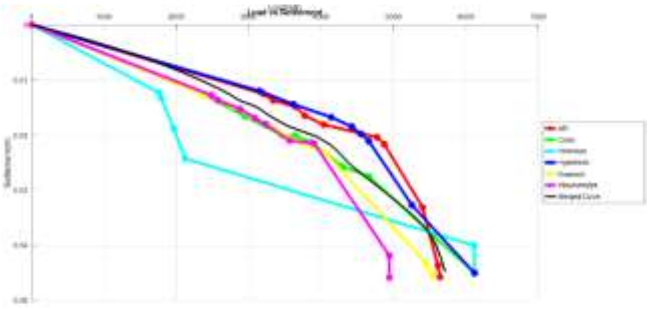

(f) Dense Sand

**Fig 2.** Composite Curve for various soils

In Figure 2a, it can be seen that when a load is applied to uniform soil, the settlement increases gradually as the soil compresses. During this phase, the soil particles rearrange themselves, and the voids between particles decrease. This phase is largely elastic, where the soil is able to recover somewhat if the load is removed. After a certain load threshold (in this case, around 1000 kN), the soil may enter a plastic deformation phase. This is where the soil experiences yielding or plastic behavior, meaning the particles start to slide or move relative to each other, causing a sharp increase in settlement. This could be due to the soil may have reached its elastic limit, and further load causes plastic deformation or shear failure. When load increases quickly, the pore water in saturated soils may not drain fast enough, leading to a temporary increase in pore pressure and a corresponding sharp settlement. After the sharp settlement increase, the rate of settlement slows down, indicating the system is stabilizing. This could be because in cohesive soils, after a certain load, the excess pore water pressure may start dissipating, and the soil begins to consolidate slowly over time, which reduces the rate of settlement. The soil might have compacted to a point where further load causes smaller incremental settlements, as the particles are already tightly packed. In some soils, after the initial yielding, the soil may exhibit strain hardening, where it becomes denser and more resistant to further deformation. This pattern of behavior is typical in non-linear soil settlement under high loads and is influenced by factors like soil type (cohesive or granular), moisture content, drainage conditions, and load application rate.

This study has several technical advantages in terms of analyzing load vs. settlement behavior for various soil types, and it contributes to more accurate and reliable geotechnical design. By combining the results from multiple studies and assigning weightage based on conservatism (i.e., which study provides a more reliable or safer value), this study created a composite load-settlement curve that incorporates the best aspects of each study. This makes the final curve more robust, as it reflects a broader range of experimental data and methodologies, reducing the chances of over- or under-estimating settlement under load. Since the study identified and weighted the more conservative studies (those that predict safer, lower allowable loads), the final load vs. settlement curve is inherently conservative. This is crucial in geotechnical design because it ensures that the soil's bearing capacity is not overestimated, leading to safer foundation designs. Conservative design means lower risks of excessive settlement, structural damage, or failure.

Soil behavior under load can be highly variable due to the complex nature of soil mechanics and differences in soil type, moisture content, and compaction. By combining curves from multiple studies, this study effectively averaging out the variability in the data and reducing the uncertainty in load-settlement predictions. This provides a more reliable basis for foundation design decisions, especially when the soil properties are uncertain or heterogeneous. Each soil type and condition may capture a different aspect of the soil's response to loading, such as elastic deformation, plastic deformation, and consolidation behavior. By combining these studies into a single curve, this study generating a more holistic representation of soil behavior, which can be more applicable in real-world scenarios where the soil profile is often non-uniform. By assigning weightage to each study based on its conservatism and relevance, anyone can customize the final curve to the specific needs of a project. For example, in cases where safety is more critical, more weight can be given to the more conservative studies, while in other cases, where a higher allowable load may be acceptable, the weighting can be adjusted accordingly. Having a combined load-settlement curve helps in making better-informed decisions for foundation design, whether it's shallow foundations or deep foundations (piles, caissons). It allows designers to more accurately determine the allowable load and predict settlement at different stages of loading, which can help in optimizing the design of foundations to avoid over-designing (which can be costly) or under-designing (which can lead to failure). The method of combining multiple curves based on weightage can be easily adapted to other types of soils or conditions. If new studies or data sets become available, they can be incorporated into the analysis, and the combined curve can be recalculated. This adaptability ensures that the model remains up-to-date and relevant as more data is collected. Since different studies might capture different load ranges more accurately (e.g., lower loads vs. higher loads), combining curves allows for a more accurate understanding of soil behavior across a wide range of loads. This can be crucial for projects where the load varies significantly (such as in large buildings or infrastructure).

## IV. CONCLUSIONS

This research presents an in-depth analysis of six distinct methods—Point by Point Curve, Cubic Root Curve, Hirayama Curve, Hyperbolic Curve, Krasinski Curve, and Root Curve—applied to evaluate the allowable load for pile foundations under various conditions. The performance of each method was assessed in terms of load-settlement behavior, aiming to determine the most conservative and reliable approach for pile design. Based on the results outlined in Table VI, it was observed that each method offers unique insights into allowable load estimation, but the Hirayama Curve consistently demonstrated a more conservative design, as it yielded the minimum allowable load. This conservative nature translates into a higher factor of safety, making the Hirayama Curve a preferred choice when prioritizing structural safety and stability in pile foundation designs. A major contribution of this study is the development of a merged curve, which combines the strengths and individual characteristics of the six evaluated methods. Each curve contributes its unique parameters, such as load-bearing capacities and settlement behaviors, creating a comprehensive load-settlement relationship that is applicable across a wider range of conditions. This merged curve effectively synthesizes the qualities of the individual methods, offering an enhanced model that provides reliable load vs. settlement predictions for different soil types and pile dimensions.

The merged curve is designed to account for six types of soil conditions and five classes of pile dimensions, making it a versatile tool for structural engineers. It offers significant practical value by allowing for more accurate predictions of pile performance under varied geological and design constraints. The integration of the six methods into a single model also provides a novel approach to pile foundation design, as it allows the flexibility to adapt to specific project requirements while maintaining the robustness of established methods. In summary, the findings of this research show that the Hirayama Curve is the most conservative and provides a higher factor of safety compared to the other methods. Additionally, the creation of the merged curve represents a significant innovation, combining the best features of the six individual methods. This merged model can be used to optimize pile design for a wide range of soil conditions and pile dimensions, providing engineers with a powerful tool for improving the safety, reliability, and efficiency of pile foundation designs. Consequently, the outcomes of this study are expected to contribute to more informed decision-making in structural design, particularly in complex soil environments. This study delivers important insights and a refined approach for geotechnical engineers and foundation designers, enabling more precise assessment of pile capacities and optimizing pile design methodologies. Future investigations should aim to expand the scope by including a broader array of pile types and additional parameters, thus enhancing both the accuracy and practicality of the proposed techniques.

## DATA AVAILABILITY STATEMENT

The sample data collection sheet and the data used for analysis, along with the associated computer programs, can be available on request from the corresponding author.

## REFERENCES


1. Dutta, S. C., & Roy, R. (2002). A critical review on idealization and modeling for interaction among soil–foundation–structure system. Computers & Structures, 80(20-21), 1579-1594.
2. Reese, L. C., Isenhower, W. M., & Wang, S. T. (2005). Analysis and design of shallow and deep foundations, 10, John Wiley & Sons.
3. Kempfert, H. G., & Gebreselassie, B. (2006). Pile foundation. Excavations and Foundations in Soft Soils, 349-460.
4. Meyerhof, G. G. (1976). Bearing capacity and settlement of pile foundations. Journal of the Geotechnical Engineering Division, 102(3), 197-228.
5. Mattes, N. S., & Poulos, H. G. (1969). Settlement of single compressible pile. Journal of the Soil Mechanics and Foundations Division, 95(1), 189-207.
6. Poulos, H. G., & Davis, E. H. (1980). Pile foundation analysis and design (Vol. 397, pp. 233-248). New York: Wiley.
7. Hirayama, H. (1988). A unified base bearing capacity formula for piles. Soils and Foundations, 28(3), 91-102.
8. Zhu, H., & Chang, M. F. (2002). Load transfer curves along bored piles considering modulus degradation. Journal of Geotechnical and Geoenvironmental Engineering, 128(9), 764-774.
9. Coyle, H. M., & Reese, L. C. (1966). Load transfer for axially loaded piles in clay. Journal of the Soil Mechanics and Foundations Division, 92(2), 1-26.
10. Coyle, H. M., & Sulaiman, I. H. (1967). Skin friction for steel piles in sand. Journal of the Soil Mechanics and Foundations Division, 93(6), 261-278.
11. Guo, W. D., & Randolph, M. F. (1998). Rationality of load transfer approach for pile analysis. Computers and Geotechnics, 23(1-2), 85-112.
12. Vijivergiya, V. N. (1977). Load-movement characteristics of piles. In 4th Symp. of Waterway, Port, Coastal and Ocean Div., ASCE (Vol. 2, pp. 269-284).
13. Verbrugge, J. C. (1981). Évaluation du tassement des pieux à partir de l'essai de pénétration statique. Revue Française de Géotechnique, (15), 75-82.
14. Frank, R., & Zhao, S. R. (1982). Estimating the settlement of axially loaded bored piles in fine sand by PMT data. Bull. Liaison LPC, 119.
15. Frank, R. (1985). Recent developments in the prediction of pile behavior from pressuremeter tests. From theory to practice on deep foundations, UFRGS, Porto Alegre, Brazil.
16. Hirayama, H. (1990). Load-settlement analysis for bored piles using hyperbolic transfer functions. Soils and Foundations, 30(1), 55-64.
17. American Petroleum Institute (API). (1993). Recommended practice for planning, designing, and constructing fixed offshore platforms–Working stress design, 20th Ed., Washington, DC.
18. Bohn, C., Lopes dos Santos, A., & Frank, R. (2017). Development of axial pile load transfer curves based on instrumented load tests. Journal of Geotechnical and Geoenvironmental Engineering, 143(1), 04016081.
19. Randolph, M. F., & Wroth, C. P. (1978). Analysis of deformation of vertically loaded piles. Journal of the Geotechnical Engineering Division, 104(12), 1465-1488.
20. Briaud, J. L., & Tucker, L. (1984). Piles in sand: a method including residual stresses. Journal of Geotechnical Engineering, 110(11), 1666-1680.
21. Chow, Y. K. (1987). Axial and lateral response of pile groups embedded in nonhomogeneous soils. International Journal for Numerical and Analytical Methods in Geomechanics, 11(6), 621-638.
22. Poulos, H. G. (1987). Analysis of residual stress effects in piles. Journal of Geotechnical Engineering, 113(3), 216-229.
23. Polo, J. M., & Clemente, J. L. (1988). Pile-group settlement using independent shaft and point loads. Journal of Geotechnical Engineering, 114(4), 469-487.
24. Kiousis, P. D., & Elansary, A. S. (1987). Load settlement relation for axially loaded piles. Journal of Geotechnical Engineering, 113(6), 655-661.
25. Kaniraj, S. R. (1993). A semi-empirical equation for settlement ratio of pile foundations in sand. Soils and Foundations, 33(2), 82-90.
26. Zhu, H., & Chang, M. F. (2002). Load transfer curves along bored piles considering modulus degradation. Journal of Geotechnical and Geoenvironmental Engineering, 128(9), 764-774.
27. Bohn, C., Lopes dos Santos, A., & Frank, R. (2017). Development of axial pile load transfer curves based on instrumented load tests. Journal of Geotechnical and Geoenvironmental Engineering, 143(1), 04016081.
28. Zhou, Z., Zhang, Z., Chen, C., Xu, F., Xu, T., Zhu, L., & Liu, T. (2022). Application of load transfer method for bored pile in loess area. European Journal of Environmental and Civil Engineering, 26(10), 4457-4475.
29. Balakrishnan, E. G., Balasubramaniam, A. S., & Phien-wej, N. (1999). Load deformation analysis of bored piles in residual weathered formation. Journal of Geotechnical and Geoenvironmental Engineering, 125(2), 122-131.
30. Kim, S., Jeong, S., Cho, S., & Park, I. (1999). Shear load transfer characteristics of drilled shafts in weathered rocks. Journal of Geotechnical and Geoenvironmental Engineering, 125(11), 999-1010.
31. Shen, W. Y., Chow, Y. K., & Yong, K. Y. (2000). A variational approach for the analysis of pile group–pile cap interaction. Geotechnique, 50(4), 349-357.
32. Dyson, G. J., & Randolph, M. F. (2001). Monotonic lateral loading of piles in calcareous sand. Journal of Geotechnical and Geoenvironmental Engineering, 127(4), 346-352.
33. Reese, L. C., Cox, W. R., & Koop, F. D. (1974). Analysis of laterally loaded piles in sand. In Offshore Technology Conference (pp. OTC-

2080). OTC.
34. O'Neill, M. W., & Murchinson, J. M. (1983). Fan evaluation of py relationships in sands. A report to the American Petroleum Institute.
35. Al-Homoud, A. S., Fouad, T., & Mokhtar, A. (2004). Evaluating accuracy for two empirical methods in predicting settlement of drilled shafts. Geotechnical & Geological Engineering, 22, 245-267.
36. Vesic, A. S. (1977). Design of pile foundations. NCHRP synthesis of highway practice, (42).
37. Mostafa, Y. E., & El Naggar, M. H. (2004). Response of fixed offshore platforms to wave and current loading including soil–structure interaction. Soil Dynamics and Earthquake Engineering, 24(4), 357-368.
38. Chang, M. F., & Zhu, H. (2004). Construction effect on load transfer along bored piles. Journal of Geotechnical and Geoenvironmental Engineering, 130(4), 426-437.
39. Kim, H. J., Mission, J. L. C., & Park, I. S. (2007). Analysis of static axial load capacity of single piles and large diameter shafts using nonlinear load transfer curves. KSCE Journal of Civil Engineering, 11, 285-292.
40. Hyeongjoo, K., Joseleo, M., Youngsun, S., Jaehong, B., & Pilsoon, B. (2008). Axial load capacity prediction of single piles in clay and sand layers using nonlinear load transfer curves. Journal of the Korean Society of Geotechnical Engineering, 24(5), 117-123.
41. Chou, Y. C., & Hsiung, Y. M. (2009). A normalized equation of axially loaded piles in elasto-plastic soil. J. Geo Eng, 4(1), 1-7.
42. Bradshaw, A. S., Haffke, S., & Baxter, C. D. (2012). Load transfer curves from a large-diameter pipe pile in silty soil. In Full-scale testing and foundation design: Honoring Bengt H. Fellenius (pp. 590-601).
43. Lim, A., Kwanda, A., & Rahardjo, P. P. (2013). The study of tz and qz curves on bored pile based on the results of instrumented pile load test in medium and stiff clays. Proceedings of Pile, 2(4th).
44. Reese, L. C., & O'NEIL, M. W. (1988). Field load tests of drilled shafts. In International Geotechnical Seminar on Deep Foundations on Bored and Auger Piles, 1 (pp. 145-191).
45. Ismail, A. (2014). Self-learning framework for estimating load transfer curves from uninstrumented pile loading tests. In Geo-Congress 2014: Geo-characterization and Modeling for Sustainability (pp. 1806-1815).
46. Nanda, S., & Patra, N. R. (2014). Theoretical load-transfer curves along piles considering soil nonlinearity. Journal of Geotechnical and Geoenvironmental Engineering, 140(1), 91-101.
47. Abchir, Z., Burlon, S., Frank, R., Habert, J., & Legrand, S. (2016). t–z curves for piles from pressuremeter test results. Géotechnique, 66(2), 137-148.
48. Grecu, S., Barari, A., & Ibsen, L. B. (2019). Axial load-transfer curves for suction bucket foundations in sand. In ISOPE International Ocean and Polar Engineering Conference (pp. ISOPE-I). ISOPE.
49. Octave, G. N. U. (2008). A high-level language, primarily intended for numerical computations, version 3.0. 3.
50. Rezaei, J., (2015). Best-worst multi-criteria decision-making method. Omega 53,49–57
51. Gerwick, B. C., & Brauner, H. A. (1978). Design of high-performance prestressed concrete piles for dynamic loading. Behavior of deep foundations, 323-334.
52. Mohammadi, A., Ebadi, T., Eslami, A., & van der Zee, S. E. (2019). Axial compressive bearing capacity of piles in oil-contaminated sandy soil using FCV. Marine Georesources & Geotechnology, 37(2), 164-179.
53. Mizuno, R., Dong, L. P., Karya, A., & Nguyen, T. T. (2023, December). Design Challenges of Large Diameter and Long Steel Pipe Pile in High Plasticity Clay at Patimban Port Development Project. In International Conference on Geotechnics for Sustainable Infrastructure Development (pp. 203-220). Singapore: Springer Nature Singapore.
54. Jayasree, P. K., Arun, K. V., Oormila, R., & Sreelakshmi, H. (2018). Lateral load capacity of piles: a comparative study between indian standards and theoretical approach. Journal of The Institution of Engineers (India): Series A, 99, 587-593.
55. Liu, Z., Zhang, A., Xu, J., Zhou, C., & Zhang, L. (2021). Calculation model and bearing capacity optimization method for the soil settlement between piles in geosynthetic-reinforced pile-supported embankments based on the membrane effect. Plos one, 16(8), e0256190.
56. Lv, Y., & Zhang, D. (2018). Geometrical effects on the load transfer mechanism of pile groups: three-dimensional numerical analysis. Canadian Geotechnical Journal, 55(5), 749-757..
57. Gwizdala, K., & Krasinski, A. (2013, September). Bearing capacity of displacement piles in layered soils with highly diverse strength parameters. In Proceedings of the 18th International Conference on Soil Mechanics and Geotechnical Engineering (pp. 2-5).
58. Mascarucci, Y., Miliziano, S., & Mandolini, A. (2016). 3M analytical method: evaluation of shaft friction of bored piles in sands. Journal of Geotechnical and Geoenvironmental Engineering, 142(3), 04015086.
59. Abbas, H. O. (2021). Compressive capacity of conventional and under reamed piles in soft clay. In IOP Conference Series: Materials Science and Engineering (Vol. 1076, No. 1, p. 012094). IOP Publishing.
60. Ismael, N. F. (2001). Axial load tests on bored piles and pile groups in cemented sands. Journal of geotechnical and geoenvironmental engineering, 127(9), 766-773.
61. Krasiński, A. (2012). Proposal for calculating the bearing capacity of screw displacement piles in non-cohesive soils based on CPT results. Studia Geotechnica et Mechanica, 34(4), 41-51.
62. Greco, S., Figueira, J., & Ehrgott, M. (2016). Multiple criteria decision analysis. New York: Springer.
63. Guo, S., Zhao, H., 2017. Fuzzy best-worst multi-criteria decision-making method and its applications. Knowl.-Based Syst. 121, 23–31..
64. Abouhashem Abadi, F., Ghasemian Sahebi, I., Arab, A., Alavi, A., Karachi, H., 2018.Application of best-worst method in evaluation of medical tourism development strategy. Decis. Sci. Lett., 77–86.

## ANNEXURE I. DETAILS OF TYPICAL LENGTHS AND CAPACITIES

| Pile Type | Pile Length (m) | | Approximate Design load (kN) | |
|---|---|---|---|---|
| | Usual Range | Maximum | Usual Range | Maximum |
| Timber | 10 to 18 | 30 | 150 to 200 | 300 |
| Driven Precast Concrete | 10 to 15 | 30 | 300 to 600 | 900 |
| Driven Prestressed Concrete | 20 to 30 | 60 | 500 to 600 | 900 |
| Cast in situ concrete (Drilled Shell) | 15 to 25 | 40 | 300 to 750 | 900 |
| Concrete cast in situ bulb piles | 15 to 25 | 45 (large dia) | 600 to 3000 | 9000 (large dia) |
| Steel Pipe | 20 to 40 | Unlimited | 300 to 1000 (small dia) | 2500 to 10000 (large dia) |
| Composite | 20 to 40 | 60 | 300 to 900 | 2000 |

## ANNEXURE II: CODE FOR LOAD VS SETTLEMENT CURVE

| | | | |
|---|---|---|---|
| clc; | | deltaY3T = | fmax1 = |
| clear all; | f3 = | (((Qmid3+Q3) | K*(Gamma*(L./3))*tand(d |
| close all; | (fmax3.*Y | /2)*((L/3)*0.5 | elta); |
| B = 0.2; | T1)./(0.002 | ))/(CSA*Ep); | #disp('fmax1=') |
| L = 8 ; | 54+YT1); | Y21 = Y3new | #disp(fmax1) |
| CSA = | q3 = | + deltaY3T; | f1 = |
| ((22/7)*( | (qmax3.*Y | | (fmax1.*Y11)./(0.00254.* |
| B*B))/4; | T1)./(0.008. | fmax2 = | B+Y11); |
| SArea = | *B+YT1); | K*(Gamma*( | for i=1:ytn |
| 2*(22/7) | | L./3))*tand(de | if Y11(i)>=zs |
| *(B/2)*( | for i=1:ytn | lta); | f1(i)=fmax1; |

```
L/3);
Ep = 21000000;

Gamma = 18;

K = 2; %for section 1
Nq = 137; %for L/D = 8/0.2 and Phi = 40
delta = 30; %for section 1 #critical length = 7.5m
zs = 0.00254; %for section 2 and 1

zt = 0.1*B;% for section 3

e = 20;

#YT1=[0 0.05 0.1 0.15 0.2 0.25];
YT1=[0 0.0001 0.0005 0.0007 0.001 0.005 0.01];
#YT1=[0 0.000001 0.000003
```

```
  if YT1(i)>=zt

    q3(i)=qmax3;
  end
  if YT1(i)>=zs

    f3(i)=fmax3;
  end
end
#disp('Point resistance =');
#disp(q3)
#disp('f3=');
#disp(f3)
T3=q3*CSA;
Q3 = T3 + (f3*SArea); %Load at the top of the bottom segment
#disp('Q3=')
#disp(Q3)
Qmid3 = (Q3 + T3)/2;
deltaY3B = (((Qmid3+T3)/2)*((L/3)*0.5))/(CSA*Ep);
Y3new = YT1 + deltaY3B;
for i=1:ytn

  error(i)=abs(((Y3new(i)-YT1(i))/YT1(i))*100); % in percentage
```

```
f2 = (fmax2.*Y21)./(0.00254.*B+Y21);
for i=1:ytn
  if Y21(i)>=zs

    f2(i)=fmax2;
  end
end
#disp('f2=');
#disp(f2)
Q2 = Q3 + (f2*SArea); %Load at the top of the bottom segment
#disp('Q2=')
#disp(Q2)
Qmid2 = (Q2 + Q3)/2;
deltaY2B = (((Qmid2+Q3)/2)*((L/3)*0.5))/(CSA*Ep);
Y2new = Y21 + deltaY2B;
for i=1:ytn

  error(i)=abs(((Y2new(i)-Y21(i))/Y21(i))*100); % in percentage
end
for i=1:ytn
  while (error(i)>=e)

    Y21(i)=Y2new(i);

    f2(i)=fmax2*((2*sqrt(Y2new(i)/zs))-(Y2new(i)/zs));
```

```
  end
end
#disp('f1=');
#disp(f1)
Q1 = Q2 + (f1*SArea); %Load at the top of the bottom segment
#disp('Q1=')
disp(Q1)
Qmid1 = (Q1 + Q2)/2;
deltaY1B = (((Qmid1+Q2)/2)*((L/3)*0.5))/(CSA*Ep);
Y1new = Y11 + deltaY1B;
for i=1:ytn
  error(i)= abs(((Y1new(i)-Y11(i))/Y11(i))*100); % in percentage
end
for i=1:ytn
  while (error(i)>=e)
    Y11(i)=Y1new(i);

    f1(i)=fmax1*((2*sqrt(Y1new(i)/zs))-(Y1new(i)/zs));

    Q1(i)=Q2(i)+(f1(i)*SArea);

    Qmid1(i) = (Q1(i)+Q2(i))/2;
    deltaY1B(i) = (((Qmid1(i)+Q2(i))/2)*((L/3)*0.5))/(CSA*Ep);
    Y1new(i) = Y11(i)+deltaY1B(i);
    error(i)=abs(((Y1new(i)-Y11(i))/Y11(i))*100);
  end
end
#disp('Y1new=');
#disp(Y1new)
deltaY1T = (((Qmid1+Q1)/2)*((L/3)*0.5))/(CSA*Ep);
Y1 = Y1new + deltaY1T;
#disp('Y1=');
disp(Y1)
disp(Q1)
plot(Y1,Q1)
```

```
0.000005];
#YT1=[0 .0018]
ytn=length(YT1);
fmax3 = K*(Gamma*(L./3))*tand(delta);
#disp('fmax3=');
#disp(fmax3)
qmax3 = (Gamma*12)*Nq;
```

```
end
for i=1:ytn
  while (error(i)>=e)

    YT1(i)=Y3new(i);

    f3(i)=fmax3*((2*sqrt(Y3new(i)/zs))-(Y3new(i)/zs));

    Q3(i)=T3(i)+(f3(i)*SArea);
    Qmid3(i) = (Q3(i)+T3(i))/2;

    deltaY3B(i) = (((Qmid3(i)+T3(i))/2)*((L/3)*0.5))/(CSA*Ep);
    Y3new(i) = YT1(i)+deltaY3B(i);

    error(i)=abs(((Y3new(i)-YT1(i))/YT1(i))*100);
  end
end
```

```
Q2(i)=Q3(i)+(f2(i)*SArea);
    Qmid2(i) = (Q2(i)+Q3(i))/2;
    deltaY2B(i) = (((Qmid2(i)+Q3(i))/2)*((L/3)*0.5))/(CSA*Ep);
    Y2new(i) = Y21(i)+deltaY2B(i);

    error(i)=abs(((Y2new(i)-Y21(i))/Y21(i))*100);
  end
end
#disp('Y2new=');
#disp(Y2new)
deltaY2T = (((Qmid2+Q2)/2)*((L/3)*0.5))/(CSA*Ep);
Y11 = Y2new + deltaY2T;
```

**ANNEXURE III: PREFERENCE OF THE BEST AND WORST CRITERION OVER THE OTHER CRITERIA FOR SILTY SOIL (B=0.5M AND L=12M).**

The preference of the best criterion over the other criteria should be assessed using a scale from 1 to 9, where

1 signifies equal preference, and 9 indicates a strong preference. The preferences can be represented as follows.

| BEST | S3 | S1 | S2 | S4 | S5 | S6 |
|---|---|---|---|---|---|---|
| *Hirayama curve* | 1 | 8 | 5 | 7 | 3 | 4 |

Similarly, the preference of the worst criterion over the other criteria should be evaluated using a scale from 1 to 9, where 1 represents equal preference and 9 signifies strong preference.

| WORST | *Point by point curves* |
|---|---|
| **Hirayama curve** | 9 |
| **Point by point curves** | 1 |
| **Cubic root curve** | 3 |
| **Hyperbolic curve** | 2 |
| **Krasinski** | 4 |
| **Root curve** | 3 |

## Author Profile

**KALITA GITARTHA**
Civil Engineer, Public Works Department (PWD), Buildings and National Highways Division.

**Dr. PALASH JYOTI HAZARIKA**
Professor & Head, Civil Engineering Department, Assam Engineering College, Guwahati.